

New Heavy Exotic Hadrons

Chengping Shen^{*†}

Graduate School of Science, Nagoya University, Nagoya, Japan

E-mail: shencp@phys.hawaii.edu

We review recent studies on exotic states at the Belle experiment. The results include: (1) The measurement of the cross sections of $\gamma\gamma \rightarrow \omega\phi$, $\phi\phi$, and $\omega\omega$ for masses that range from threshold to 4.0 GeV. In addition to signals from well established spin-zero and spin-two charmonium states, there are clear resonant structures below charmonium threshold, which have not been previously observed. We report a spin-parity analysis for the new structures; (2) No $X(3872)$ signal is observed in $\eta J/\psi$ or $\gamma\chi_{c1}$ mode in B decays. A narrow peak at $3823.5 \text{ MeV}/c^2$ (named as ψ_2) to $\gamma\chi_{c1}$ with a significance of 4.2 standard deviations including systematic uncertainty is observed in $B^\pm \rightarrow K^\pm \gamma\chi_{c1}$; (3) The bottomonium states $h_b(1P)$, $h_b(2P)$ and $Y(1D)$ are observed in the reaction $e^+e^- \rightarrow \pi^+\pi^- + X$; (4) The observation of two narrow charged structures (named as $Z_b(10610)$ and $Z_b(10650)$) in the mass spectra of the $\pi^\pm Y(nS) (n = 1, 2, 3)$ and $\pi^\pm h_b(mP) (m = 1, 2)$ pairs that are produced in association with a single charged pion in $Y(5S)$ decays.

Sixth International Conference on Quarks and Nuclear Physics,

April 16-20, 2012

Ecole Polytechnique, Palaiseau, Paris

^{*}Speaker.

[†]On behalf of the Belle collaboration and supported by a Grant-in-Aid for Scientific Research on Innovative Areas “Elucidation of New Hadrons with a Variety of Flavors” from the ministry of Education, Culture, Sports, Science and Technology of Japan and a Grant-in-Aid for Young Scientists (B) under contract 24740158.

1. Introduction

In hadronic physics, the best understood quark-antiquark systems are heavy quarkonia, i.e., $c\bar{c}$ or $b\bar{b}$ mesons. The discovery of the missing $c\bar{c}$ or $b\bar{b}$ states and the precise measurements of properties of the already observed ones are important.

The QCD-motivated models predict the existence of hadrons of more complex structure than conventional mesons or baryons, such as hybrids, multiquark states of either molecular, tetraquark or hadrocharmonium configuration. As the conventional hadron spectrum is much cleaner than the dense spectrum of light states, exotic states containing $c\bar{c}$ or $b\bar{b}$ are expected to be identified more easily than the ones predicted in the light spectrum. Any resonance observed in addition to predicted multiplets might give a hint of such an exotic spectroscopy.

Some of the recently observed charmonium-like or bottomonium-like XYZ states could be candidates for the exotic hadrons mentioned. However most of them still await confirmation or their properties need to be further studied before any decisive interpretation is made. Here, we review some recent results on the exotic hadrons from Belle experiment.

2. Observation of new resonant structures in $\gamma\gamma \rightarrow \omega\phi$, $\phi\phi$ and $\omega\omega$

Recently a clear signal for a new state $X(3915) \rightarrow \omega J/\psi$ [1] and evidence for another state $X(4350) \rightarrow \phi J/\psi$ [2] have been reported, thereby introducing new puzzles to charmonium or charmonium-like spectroscopy. It is natural to extend the above theoretical picture to similar states coupling to $\omega\phi$, $\omega\omega$ or $\phi\phi$.

The measurements of the cross sections for $\gamma\gamma \rightarrow VV$ [3], where $VV = \omega\phi, \phi\phi$ and $\omega\omega$, are based on an analysis of an 870 fb^{-1} data sample taken at or near the $\Upsilon(nS)$ ($n = 1, \dots, 5$) resonances with the Belle detector operating at the KEKB asymmetric-energy e^+e^- collider.

After event selections, clear ω or ϕ signal is observed. The magnitude of the vector sum of the final particles' transverse momenta in the e^+e^- center-of-mass (C.M.) frame, $|\sum \vec{P}_t^*|$, which approximates the transverse momentum of the two-photon-collision system, is used as a discriminating variable to separate signal from background. We obtain the number of VV events in each VV invariant mass bin by fitting the $|\sum \vec{P}_t^*|$ distribution between zero and $0.9 \text{ GeV}/c$. The resulting VV invariant mass distributions are shown in Fig. 1, where there are some obvious structures in the low VV invariant mass region.

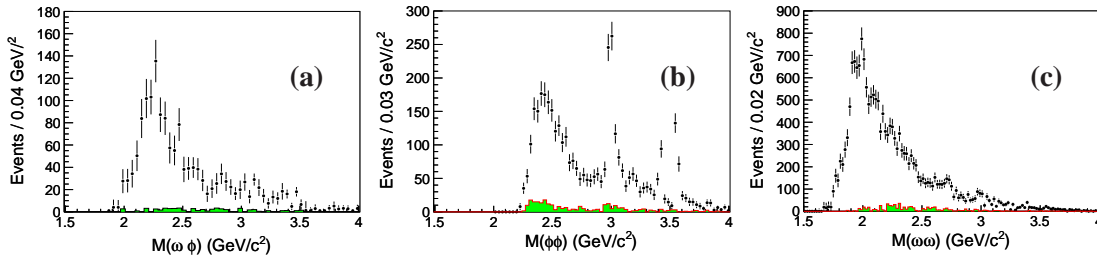


Figure 1: The (a) $\omega\phi$, (b) $\phi\phi$ and (c) $\omega\omega$ invariant mass distributions. The shaded histograms are from the corresponding normalized sidebands, which will be subtracted in calculating the final cross sections.

Two-dimensional (2D) angular distributions are investigated to obtain the J^P of the structures. In the process $\gamma\gamma \rightarrow VV$, five angles are kinematically independent. We choose z , z^* , z^{**} , ϕ^* , and

ϕ^{**} [4] and use the transversity angle (ϕ_T) and polar-angle product (Π_θ) variables to analyze the angular distributions. They are defined as $\phi_T = |\phi^* + \phi^{**}|/2\pi$, $\Pi_\theta = [1 - (z^*)^2][1 - (z^{**})^2]$.

We obtain the number of signal events by fitting the $|\sum \vec{P}_i^*|$ distribution in each ϕ_T and Π_θ bin in the 2D space, which is divided into 4×4 , 5×5 , and 10×10 bins for $\omega\phi$, $\phi\phi$, and $\omega\omega$, respectively, for $M(VV) < 2.8 \text{ GeV}/c^2$, in some wider VV mass bins as shown in Fig. 2. The obtained 2D angular distribution data are fitted with the signal shapes from MC-simulated samples with different J^P assumptions (0^+ , 0^- , 2^+ , 2^-). We find: (1) for $\omega\phi$: 0^+ (S-wave) or 2^+ (S-wave) can describe data with $\chi^2/ndf = 1.1$ or 1.2, while a mixture of 0^+ (S-wave) and 2^+ (S-wave) describes data with $\chi^2/ndf = 0.9$ (ndf is the number of degrees of freedom); (2) for $\phi\phi$: a mixture of 0^+ (S-wave) and 2^- (P-wave) describes data with $\chi^2/ndf = 1.3$; and (3) for $\omega\omega$: a mixture of 0^+ (S-wave) and 2^+ (S-wave) describes data with $\chi^2/ndf = 1.3$.

The $\gamma\gamma \rightarrow VV$ cross sections are shown in Fig. 2. The cross sections for different J^P values as a function of $M(VV)$ are also shown in Fig. 2. While there are substantial spin-zero components in all three modes, there are also significant spin-two components, at least in the $\phi\phi$ and $\omega\omega$ modes.

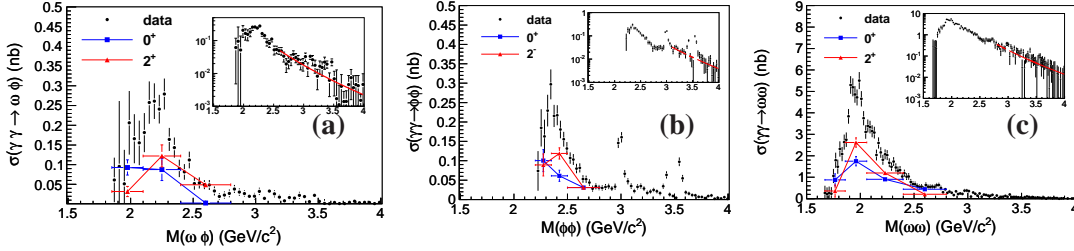


Figure 2: The cross sections of $\gamma\gamma \rightarrow \omega\phi$ (a), $\phi\phi$ (b), and $\omega\omega$ (c) are shown as points with error bars. The cross sections for different J^P values as a function of $M(VV)$ are shown as the triangles and squares with error bars. The inset also shows the cross section on a semi-logarithmic scale. In the high energy region, the solid curve shows a fit to a $W_{\gamma\gamma}^{-n}$ dependence for the cross section after the significant charmonium contributions (η_c , χ_{c0} and χ_{c2}) were excluded.

The cross sections for $\gamma\gamma \rightarrow \omega\phi$ are much lower than the prediction of the $q^2\bar{q}^2$ tetraquark model [5] of 1 nb, while the resonant structure in the $\gamma\gamma \rightarrow \phi\phi$ mode is nearly at the predicted position. However, the $\phi\phi$ cross section is an order of magnitude lower than the expectation in the tetraquark model. On the other hand, the t-channel factorization model [6] predicted that the $\phi\phi$ cross sections vary between 0.001 nb and 0.05 nb in the mass region of 2.0 GeV/c^2 to 5.0 GeV/c^2 , which are much lower than the experimental data. For $\gamma\gamma \rightarrow \omega\omega$, the t-channel factorization model [6] predicted a broad structure between 1.8 GeV/c^2 and 3.0 GeV/c^2 with a peak cross section of 10-30 nb near 2.2 GeV/c^2 , while the one-pion-exchange model [7] predicted an enhancement near threshold around 1.6 GeV/c^2 with a peak cross section of 13 nb using a preferred value of the slope parameter. Both the peak position and the peak height predicted in [6] and [7] disagree with our measurements.

3. Charmonium and charmonium-like states

If $X(3872)$ is a tetraquark state, then it has a C -odd parity ($C = -$) partner, which can dominantly decay into $J/\psi\eta$ and $\chi_{c1}\gamma$. $B^\pm \rightarrow (J/\psi\eta(\rightarrow \gamma\gamma))K^\pm$ and $B^\pm \rightarrow (\chi_{c1}(\rightarrow J/\psi\gamma)\gamma)K^\pm$ decay

modes are used in the search for C -odd partner of the $X(3872)$ and other new narrow resonances. In all the decay modes, J/ψ is reconstructed via e^+e^- and $\mu^+\mu^-$. B candidates are identified using energy difference $\Delta E \equiv E_B^* - E_{beam}^*$ and beam-energy constrained mass $M_{bc} \equiv \sqrt{(E_{beam}^*)^2 - (p_B^*)^2}$, where E_{beam}^* is the beam energy in the C.M. frame, and E_B^* and p_B^* are the energy and momentum of the reconstructed particles in the C.M. frame.

The signal region for $B^\pm \rightarrow J/\psi \eta K^\pm$ candidates is defined as $M_{bc} > 5.27 \text{ GeV}/c^2$ and $-35 \text{ MeV} < \Delta E < 30 \text{ MeV}$. The final $\eta J/\psi$ invariant mass distribution is shown in Fig. 3 together with the fitted results. No hint of a narrow resonance is evident from the current statistics. No $X(3872)$ signal is seen and we obtain the limit $\mathcal{B}(B^\pm \rightarrow X(3872)K^\pm)\mathcal{B}(X(3872) \rightarrow J/\psi \eta) < 3.8 \times 10^{-6}$ at 90% C.L.

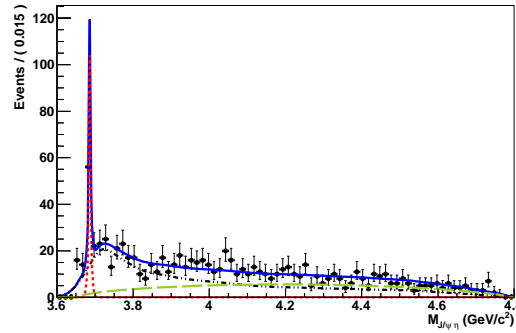


Figure 3: The fit to the $M_{J/\psi \eta}$ distribution. Red dashed (green long dashed) curve shows the signal for $B^\pm \rightarrow \psi'(\rightarrow J/\psi \eta)K^\pm$ (phase space component $B^\pm \rightarrow J/\psi \eta K^\pm$), while black dashed-dotted curve shows the background parameterized using $B \rightarrow J/\psi X$ MC sample.

Complimentary to $B^\pm \rightarrow (J/\psi \eta)K^\pm$ study, the search for the $X(3872)$'s C -odd partner is also carried in $B^\pm \rightarrow (\chi_{c1} \gamma)K^\pm$ process. Besides the $X(3872)$'s C -odd partner, we also keep an eye on any other possible narrow charmonium or charmonium-like candidate.

After all the event selections, Fig. 4 shows the $M_{\chi_{c1} \gamma}$ distribution with $M_{bc} > 5.27 \text{ GeV}/c^2$ (top left), enlarged $M_{\chi_{c1} \gamma}$ distribution (top right), M_{bc} distribution with $3.66 < M_{\chi_{c1} \gamma} < 3.708 \text{ GeV}/c^2$ (bottom left), and M_{bc} distribution with $3.805 < M_{\chi_{c1} \gamma} < 3.845 \text{ GeV}/c^2$ (bottom right). The dots with error bars are data, and the blue solid lines are the projections from 2D unbinned maximum likelihood fits. No $X(3872)$ signal is seen and the limit $\mathcal{B}(B^\pm \rightarrow X(3872)K^\pm)\mathcal{B}(X(3872) \rightarrow \gamma \chi_{c1}) < 2.0 \times 10^{-6}$ at 90% C.L. is obtained. Besides the clear ψ' signal, we find a clear evidence of a narrow peak at 3823 MeV in $M_{\chi_{c1} \gamma}$, as shown in Fig. 4 with pink dashed curve (named as $X(3823)$). The signal significance is 4.2σ with systematic error included. The mass and width of this peak are estimated to be $3823.5 \pm 2.1 \text{ MeV}/c^2$ and $4 \pm 6 \text{ MeV}$, respectively. We noticed that charmonium model predicts a narrow state ($^3D_2 c\bar{c}$) at around 3810-3840 MeV/c^2 [8]. So the $X(3823)$ is probably ψ_2 state. The measured $\mathcal{B}(B^\pm \rightarrow X(3823)K^\pm)\mathcal{B}(X(3823) \rightarrow \gamma \chi_{c1})$ is $(9.70^{+2.84+1.06}_{-2.52-1.03}) \times 10^{-6}$, where the first errors are statistical and the second systematic.

4. Bottomonium and bottomonium-like states

The spin-singlet states $h_b(nP)$ and $\eta_b(nS)$ alone provide information concerning the spin-spin

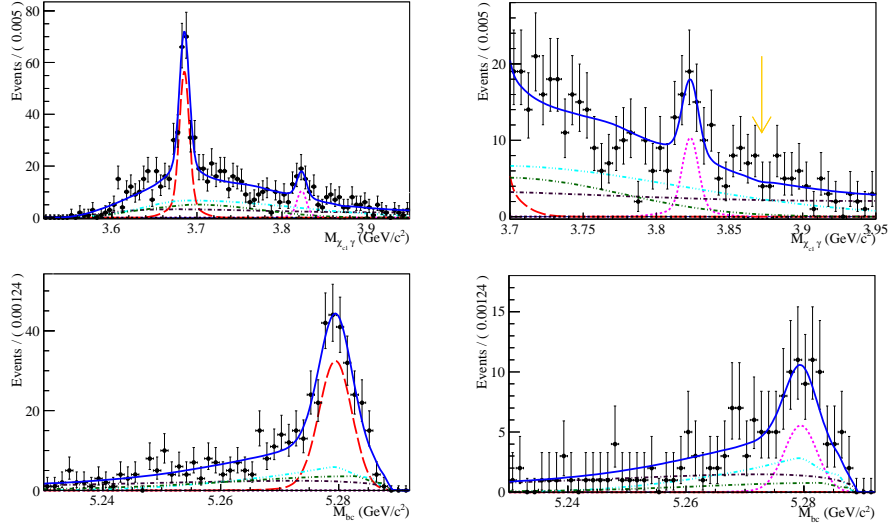


Figure 4: The projections from 2D unbinned maximum likelihood fits to the $M_{\chi_{c1}\gamma}$ distribution with $M_{bc} > 5.27 \text{ GeV}/c^2$ (top left), enlarged $M_{\chi_{c1}\gamma}$ distribution (top right, yellow arrow shows the $X(3872)$ position), M_{bc} distribution with $3.66 < M_{\chi_{c1}\gamma} < 3.708 \text{ GeV}/c^2$ (bottom left), and M_{bc} distribution with $3.805 < M_{\chi_{c1}\gamma} < 3.845 \text{ GeV}/c^2$ (bottom right). The dots with error bars are data. The blue solid line is form the overall fit. The red large-dashed and pink dashed curves are for ψ' and ψ_2 signals, respectively, while black dotted-dashed, dark green two dotted-dashed, and cyan three dotted-dashed curves are for the combinatorial background, $B^\pm \rightarrow \psi'(\text{other than } \chi_{c1}\gamma)K^\pm$ events, and peaking background component, respectively.

(or hyperfine) interaction in bottomonium. Measurements of the $h_b(nP)$ masses provide unique access to the P -wave hyperfine splitting, $\Delta M_{\text{HF}} \equiv \langle M(n^3P_J) \rangle - M(n^1P_1)$, the difference between the spin-weighted average mass of the P -wave triplet states ($\chi_{bJ}(nP)$ or n^3P_J) and that of the corresponding $h_b(nP)$, or n^1P_1 . We use a 121.4 fb^{-1} data sample collected near the peak of the $\Upsilon(5S)$ resonance ($\sqrt{s} \sim 10.865 \text{ GeV}$) with the Belle detector to report the first observation of the $h_b(1P)$ and $h_b(2P)$ produced via $e^+e^- \rightarrow h_b(nP)\pi^+\pi^-$ in the $\Upsilon(5S)$ region [9].

We observe the $h_b(nP)$ states in the $\pi^+\pi^-$ missing mass spectrum of hadronic events. The $\pi^+\pi^-$ missing mass is defined as $M_{\text{miss}}^2 \equiv (P_{\Upsilon(5S)} - P_{\pi^+\pi^-})^2$, where $P_{\Upsilon(5S)}$ is the 4-momentum of the $\Upsilon(5S)$ determined from the beam momenta and $P_{\pi^+\pi^-}$ is the 4-momentum of the $\pi^+\pi^-$ system. The $\pi^+\pi^-$ transitions between $\Upsilon(nS)$ states provide high-statistics reference signals.

To reconstruct the $\Upsilon(5S) \rightarrow h_b(nP)\pi^+\pi^-$ transitions inclusively, we use a general hadronic event selection. The M_{miss} spectrum after subtraction of both the combinatoric and $K_S^0 \rightarrow \pi^+\pi^-$ contributions is shown with the fitted signal functions overlaid in Fig. 5. The significances of the $h_b(1P)$ and $h_b(2P)$ signals, with systematic uncertainties accounted for, are 5.5σ and 11.2σ , respectively. The measured masses of $h_b(1P)$ and $h_b(2P)$ are $M = (9898.2^{+1.1}_{-1.0}) \text{ MeV}/c^2$ and $M = (10259.8 \pm 0.6^{+1.4}_{-1.0}) \text{ MeV}/c^2$, respectively. Using the world average masses of the $\chi_{bJ}(nP)$ states, we determine the hyperfine splittings to be $\Delta M_{\text{HF}} = (+1.7 \pm 1.5) \text{ MeV}/c^2$ and $(+0.5^{+1.6}_{-1.2}) \text{ MeV}/c^2$, respectively, where statistical and systematic uncertainties are combined in quadrature.

The observation of anomalously high rates for $\Upsilon(5S) \rightarrow \Upsilon(nS)\pi^+\pi^-$ ($n = 1, 2, 3$) and $\Upsilon(5S) \rightarrow h_b(nP)\pi^+\pi^-$ ($m = 1, 2$) transitions suggests that exotic mechanisms are contributing to $\Upsilon(5S)$ de-

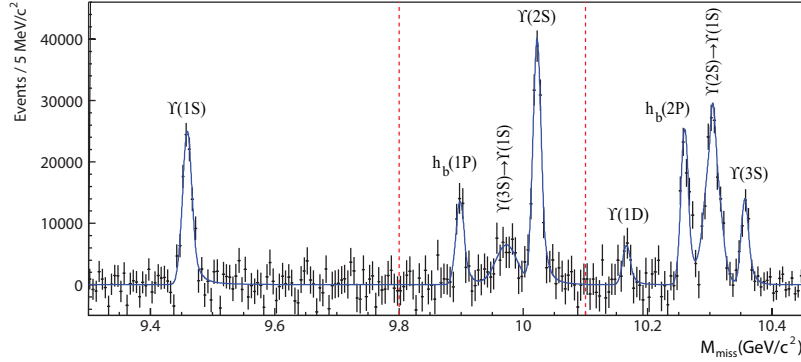


Figure 5: The inclusive M_{miss} spectrum with the combinatoric background and K_S^0 contribution subtracted (points with errors) and signal component of the fit function overlaid (smooth curve). The vertical lines indicate boundaries of the fit regions.

cays. Amplitude analyses of the three-body $\Upsilon(5S) \rightarrow \Upsilon(nS)\pi^+\pi^-$ decays with $\Upsilon(nS) \rightarrow \mu^+\mu^-$ are performed by means of unbinned maximum likelihood fits to two-dimensional $M^2[\Upsilon(nS)\pi^+]$ vs. $M^2[\Upsilon(nS)\pi^-]$ Dalitz distributions [10]. One-dimensional invariant mass projections for events in the $\Upsilon(nS)$ signal regions are shown in Fig. 6, where two peaks are observed in the $\Upsilon(nS)\pi$ system near $10.61 \text{ GeV}/c^2$ and $10.65 \text{ GeV}/c^2$ (named as $Z_b(10610)$ and $Z_b(10650)$). The combined statistical significance of the two peaks exceeds 10σ for all $\Upsilon(nS)\pi^+\pi^-$ channels.

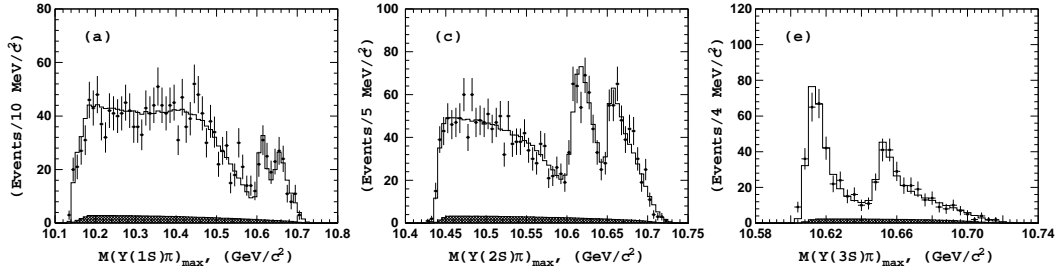


Figure 6: Comparison of fit results (open histogram) with experimental data (points with error bars) for events in the (a) $\Upsilon(1S)$, (c) $\Upsilon(2S)$, and (e) $\Upsilon(3S)$ signal regions. The hatched histogram shows the background component.

To study the resonant substructure of the $\Upsilon(5S) \rightarrow h_b(nP)\pi^+\pi^-$ ($m = 1, 2$) decays we measure their yield as a function of the $h_b(1P)\pi^\pm$ invariant mass. The decays are reconstructed inclusively using the missing mass of the $\pi^+\pi^-$ pair, M_{miss} . We fit the M_{miss} spectra in bins of $h_b(1P)\pi^\pm$ invariant mass, defined as the missing mass of the opposite sign pion, $M_{\text{miss}}(\pi^\mp)$. We combine the M_{miss} spectra for the corresponding $M_{\text{miss}}(\pi^+)$ and $M_{\text{miss}}(\pi^-)$ bins and we use half of the available $M_{\text{miss}}(\pi)$ range to avoid double counting.

The results for the yield of $\Upsilon(5S) \rightarrow h_b(nP)\pi^+\pi^-$ ($m = 1, 2$) decays as a function of the $M_{\text{miss}}(\pi)$ are shown in Fig. 7, where the fit results are shown as solid histograms. The two-peak structures are clear in both of them. The default fit hypothesis is favored over the phase-space fit hypothesis at the 18σ [6.7σ] level for the $h_b(1P)$ [$h_b(2P)$].

Weighted averages over all five channels give $M = 10607.2 \pm 2.0 \text{ MeV}/c^2$, $\Gamma = 18.4 \pm 2.4 \text{ MeV}$ for the $Z_b(10610)$ and $M = 10652.2 \pm 1.5 \text{ MeV}/c^2$, $\Gamma = 11.5 \pm 2.2 \text{ MeV}$ for the $Z_b(10650)$, where statistical and systematic errors are added in quadrature. Angular analysis favors a $J^P = 1^+$ assignment for both Z_b^+ states, which must also have negative G -parity. Transitions through Z_b^+ to the $h_b(nP)$ saturate the observed $\pi^+\pi^-h_b(nP)$ cross sections. The two masses of Z_b^+ states are just a few MeV above the $B^*\bar{B}$ and $B^*\bar{B}^*$ thresholds, respectively. The Z_b^+ cannot be simple mesons because they are charged and have $b\bar{b}$ content.

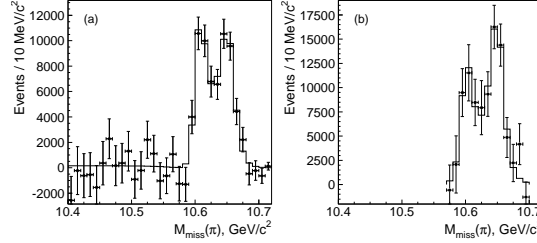


Figure 7: The (a) $h_b(1P)$ and (b) $h_b(2P)$ yields as a function of $M_{\text{miss}}(\pi)$ (points with error bars) and results of the fit (histogram).

5. Summary

We reviewed here some recent results on exotic states at the Belle experiment, including the measurement of the cross sections of $\gamma\gamma \rightarrow \omega\phi$, $\phi\phi$, and $\omega\omega$; the search for the $X(3872)$'s C-odd partner in $\eta J/\psi$ and $\gamma\chi_{c1}$ modes in B decays; the evidence of ψ_2 in $B^\pm \rightarrow K^\pm \gamma\chi_{c1}$; the observation of $h_b(1P)$, $h_b(2P)$, $Y(1D)$, and two charged $Z_b(10610)$ and $Z_b(10650)$ states.

References

- [1] S. Uehara *et al.* (Belle Collaboration), Phys. Rev. Lett. **104**, 092001 (2010).
- [2] C. P. Shen *et al.* (Belle Collaboration), Phys. Rev. Lett. **104**, 112004 (2010).
- [3] Z. Q. Liu *et al.* (Belle Collaboration), Phys. Rev. Lett. **108**, 232001 (2012).
- [4] Using $\omega\phi$ as an example, z is the cosine of the scattering polar angle of ϕ in the $\gamma\gamma$ C.M. system; z^* and ϕ^* are the cosine of the helicity angle of K^+ in the ϕ decays and the azimuthal angle defined in the ϕ rest frame with respect to the $\gamma\gamma \rightarrow \omega\phi$ scattering plane; z^{**} and ϕ^{**} are the cosine of the helicity angle of normal direction to the decay plane of the $\omega \rightarrow \pi^+\pi^-\pi^0$ and the azimuthal angle defined in the ω rest frame.
- [5] N. N. Achasov and G. N. Shestakov, Usp. Fiz. Nauk **161**, 53 (1991) [Sov. Phys. Usp. **34**, 471 (1991)].
- [6] G. Alexander, A. Levy and U. Maor, Z. Phys. C **30**, 65 (1986).
- [7] N. N. Achasov, V. A. Karnakov and G. N. Shestakov, Z. Phys. C **36**, 661 (1987).
- [8] S. Godfrey and N. Isgur, Phys. Rev. D **32**, 189 (1985); E. Eichten *et al.*, Phys. Rev. D **89**, 162002 (2002); E. Eichten *et al.*, Phys. Rev. D **69**, 094019 (2004).
- [9] I. Adachi *et al.* (Belle Collaboration), Phys. Rev. Lett. **108**, 032001 (2012).
- [10] A. Bondar *et al.* (Belle Collaboration), Phys. Rev. Lett. **108**, 122001 (2012).